Reinitiation of the Boreal Summer Intraseasonal Oscillation in the Tropical Indian Ocean*

XIAN-AN JIANG+ AND TIM LI

Department of Meteorology, and International Pacific Research Center, School of Ocean and Earth Science and Technology, University of Hawaii at Manoa, Honolulu, Hawaii

(Manuscript received 26 July 2004, in final form 8 April 2005)

ABSTRACT

The characteristic features of the boreal summer intraseasonal oscillation (BSISO) during its reinitiation period are studied using NCEP–NCAR reanalysis. Based on these observations and with the aid of an anomalous atmospheric general circulation model (AGCM), a possible mechanism responsible for the BSISO reinitiation is elucidated. The western equatorial Indian Ocean along the eastern African coast tends to be a key region for the phase transition of the BSISO from an enhanced to suppressed convective phase, or vise versa. The major precursory feature associated with reinitiation of suppressed convection is found in the divergence and reduced specific humidity in the boundary layer. Numerical experiments indicate that the low-level divergence is caused by the cold horizontal temperature advection and associated adiabatic warming (descending motion) in situ. The summer mean state is found to be important for the cold horizontal temperature advection through the modulation of a Gill-type response to an intraseasonal oscillation (ISO) heating in the eastern equatorial Indian Ocean. The results in this study suggest a self-sustained paradigm in the Indian Ocean for the BSISO; that is, the BSISO could be a basinwide phenomenon instead of a global circumstance system as hypothesized for the boreal winter ISO (i.e., the Madden–Julian oscillation).

1. Introduction

The tropical intraseasonal oscillation (ISO) exhibits pronounced seasonality (Julian and Madden 1981; Wang and Rui 1990; Hendon and Salby 1994; Hartmann et al. 1992). While being dominated by an equatorially trapped eastward-propagating mode in boreal winter (Madden and Julian 1971, 1972, 1994), the ISO is characterized by prominent northward propagation over the south Asian monsoon region during boreal summer (Yasunari 1979, 1980; Sikka and Gadgil 1980; Krishnamurti and Subrahmanyam 1982; Murakami et al. 1984; Lorenc 1984; Cadet 1986; Lau and Chan 1986; Wang and Rui 1990; Li and Wang 1994; and others). This northward propagation of boreal summer intraseasonal oscillation (BSISO) has been found to be closely associated with the active and break phases of Indian monsoon rainfall (Sikka and Gadgil 1980; Cadet 1986; Lau and Chan 1986; Gadgil and Asha 1992; Lawrence and Webster 2002) and thus has received intensive attention during past decades. For the sake of clarity, the eastward-propagating ISO mode during boreal winter season is termed as the Madden–Julian oscillation (MJO) in the following context, to be distinguished from the BSISO mode.

A number of theories have been advanced in interpreting this northward-propagating mode of the BSISO. Webster (1983) emphasized the important role of land–atmosphere interaction for the northward shift of convection, in which the land surface heat flux into the planetary boundary layer (PBL) is a key to destabilizing the atmosphere ahead of the convection. Wang and Xie (1997) and Lawrence and Webster (2002) suggested that the northward propagation of the

* School of Ocean and Earth Science and Technology Publication Number 6589 and International Pacific Research Center Publication Number 332.

+ Current affiliation: Geophysical Fluid Dynamics Laboratory, Princeton University, Princeton, New Jersey.

Corresponding author address: Dr. Xian-An Jiang, USDOC/NOAA/GFDL, P.O. Box 308, 201 Forrestal Rd., Princeton, NJ 08542.
E-mail: xianan.jiang@noaa.gov

BSISO is originated in Rossby wave emanation from the eastward-propagating equatorial Kelvin–Rossby wave packet. Kemball-Cook and Wang (2001), on the other hand, proposed that air–sea interaction could be another factor for the northward propagation of the BSISO. Strong air–sea coupling signals are also evidenced by both coupled general circulation models (GCMs; Fu et al. 2003) and observations (Sengupta and Ravichandran 2001; Sengupta et al. 2001; Bhat et al. 2001; Webster et al. 2002). Based on the analysis of both atmospheric GCM (AGCM) simulation and observations, Jiang et al. (2004) proposed two internal atmospheric dynamical mechanisms in which the vertical shear of the zonal mean flow and moisture–convection feedback are fundamental for the northward propagation.

A key question regarding the life cycle of the BSISO is how it is reinitiated. Most of the previous studies have been focused on the MJO during wintertime, and much less attention has been given to the BSISO. Regarding the reinitiation mechanisms of the MJO, there are two main theories: internal and external triggering mechanisms. For the internal triggering scenario, a previous cycle of the MJO can reinitiate new convection over the western equatorial Indian Ocean (WEIO). In this scenario, the circumnavigating Kelvin waves along the equator generated by the previously enhanced MJO convection could reinitiate new convection (Hendon 1988; Bladé and Hartmann 1993; Matthews 2000). The MJO period in this scenario could be explained by the moist Kelvin wave speed (about 15 m s^{-1}) in the presence of the wave–Convective Instability of the Second Kind (CISK; Lau and Peng 1987; Chang and Lim 1988) or Ekman–CISK (Chang 1977; Wang and Rui 1990; Wang and Li 1994).

Bladé and Hartmann (1993) suggested that the MJO period is set by the growth and duration times of the convective episode together with the recharge time for the instability. Hu and Randall (1994) suggested that the reinitiation of convection near the equator in the Indian Ocean is a result of self-adjustment of a stationary heat source by the nonlinear interaction among radiation, convection, and surface moisture flux.

Matthews (2000) proposed that the reinitiation of suppressed convection over the WEIO could be induced by the divergence due to the decrease in the strength of the westerly wind anomalies to the west of the enhanced convection over the eastern equatorial Indian Ocean (EEIO). By this mechanism, it was suggested that successive cycles of the MJO can be generated locally within the warm-pool region. Hsu and Lee (2005) proposed that the lifting and frictional effects of the tropical topography may be essential for the reinitiation of the new convection on the east side of the mountains with the presence of the equatorial Kelvin waves, which are excited by the deep heating anomalies on the west side. Seo and Kim (2003) suggested that the interaction of Kelvin and Rossby waves plays an important role in reinitiating a new cycle of the MJO. The Kelvin waves generated by the enhanced convection anomaly of the previous cycle and the Rossby wave response to the reduced convection anomaly of the current cycle over the Indian Ocean appear to generate a new cycle of the MJO over the WEIO.

Another theory for the reinitiation of the MJO convection emphasizes the external triggering mechanism associated with the penetration of the midlatitude Rossby waves (Hsu et al. 1990) or energy dispersion from baroclinic eddies (Bladé and Hartmann 1993; Slingo et al. 1999; Matthews and Kiladis 1999). However, little evidence of systematic reinitiation of convection by the incursion of extratropical waves into the Indian Ocean was shown in the composite of the 200-mb streamfunction field (Kemball-Cook 1999).

Most of the hypotheses above are aimed to explain the reinitiation of the wintertime MJO. However, the frequency and movement of the observed ISO exhibit significant seasonality. In contrast to the strong eastward propagation of the MJO during boreal winter, globally propagating equatorial Kelvin waves associated with the BSISO have not been evidenced even in the upper-tropospheric circulation. This implies that the triggering mechanism for the ISO during boreal summer may differ from that in boreal winter.

The present study is devoted to improved understanding for the characteristics of and physical mechanisms for the BSISO reinitiation. The organization of this paper is as follows. The descriptions of the dataset and numerical model employed in this study will be presented in section 2. In section 3, we attempt to reveal the characteristic features of the BSISO during its reinitiation process based on the observations. Then a physical mechanism responsible for the reinitiation of the BSISO will be illustrated based on an AGCM simulation in section 4. In section 5, this proposed mechanism is to be further verified with the observations. Finally, a summary and discussion will be presented.

2. Data and model

a. Data

The primary datasets used for this study are the National Oceanic and Atmospheric Administration (NOAA) outgoing longwave radiation (OLR; Lieb-

mann and Smith 1996) and the National Centers for Environmental Prediction–National Center for Atmospheric Research (NCEP–NCAR) reanalysis (Kalnay et al. 1996). Both of the datasets are daily averaged with $2.5° \times 2.5°$ global coverage. The OLR is used as a proxy for the deep tropical convection, and variables by the NCEP–NCAR reanalysis include the multilevel zonal and meridional wind components (12 vertical pressure levels from 1000 to 100 mb), specific humidity (9 vertical levels from 1000 to 300 mb), and surface latent heat flux. Based on these datasets, ISOs during the summer seasons for the period from 1980 to 2001 are examined.

b. Princeton AGCM

A dry version of the Princeton AGCM is employed for this study (Held and Suarez 1994). This global spectral model uses sigma ($\sigma = p/p_s$) as its vertical coordinate. The basic equations include momentum, temperature, and logarithm of surface pressure equations together with the diagnostic equation for the vertical velocity, the detailed expression of which can be found in the appendix.

In the present study, this model is linearized by a specified 3D summer mean [June–August (JJA)] basic state in a way similar with that used by Ting and Yu (1998), so that one may examine how the atmosphere responds to a specific anomalous heating in the presence of an idealized or realistic mean state. The perturbation equations retain full nonlinearity. The model atmosphere is formulated with five evenly distributed sigma levels with an interval of 0.2, a top level at $\sigma = 0$, and a bottom level at $\sigma = 1$. The horizontal resolution of T42 is adopted in this study. The same biharmonic diffusion is applied to momentum and temperature equations with a dissipating rate of 0.1 day^{-1} for the smallest resolvable scale in this model. Rayleigh friction is applied to the momentum equations, with the damping rate of 1 day^{-1} taken in the lowest model level ($\sigma = 0.9$) to mimic the planetary boundary layer, then linearly decaying to 0.1 day^{-1} at the level of $\sigma = 0.7$. Newtonian cooling with an *e*-folding time scale of 10 days is applied to the temperature equation at all the model levels.

In this study, we intend to employ this model to examine the tropical atmospheric response to a prescribed ISO heating in the presence of the 3D summer mean flow. To intentionally exclude the impact of midlatitude perturbation, a strong dynamical and thermal damping of 1 day^{-1} is applied in momentum and temperature equations for the off-tropical region beyond 40°N and 40°S. A realistic summer (JJA) mean state is prescribed as the model basic state, which is taken from the long time mean of the NCEP–NCAR reanalysis by linearly interpolating the original pressure surface data to the five sigma levels. The model is integrated for 20 days to get the equilibrium state.

By using this model, Wang et al. (2003) demonstrated that the observed low-level anticyclonic circulation over the south Asian monsoon region during the summer of an ENSO-developing year can be ascribed to the equatorial Rossby wave response to a heat sink over the Maritime Continent, which is greatly modulated by the monsoonal mean flow.

3. Circulation features associated with the BSISO reinitiation

A method based on EOF analysis is first employed to measure the intensity of individual BSISO events. EOF analysis has been widely employed to extract the dominant modes of ISO convection (e.g., Lau and Chan 1986; Ferranti et al. 1990; Zhang and Hendon 1997; Hendon et al. 1999; Lawrence and Webster 2001). Before performing the EOF analysis, the daily OLR data as well as other variables, including 3D winds, vertical velocity, specific humidity, and surface latent heat flux at each grid point within the domain of 15°S–30°N, 40°E–180° during the 22-yr period (1980–2001), were subject to a 20–70-day bandpass filtering based on the harmonic decomposition (Kemball-Cook and Wang 2001; Teng and Wang 2003; Jiang et al. 2004). Then the filtered OLR data from May to September of each year were used for the EOF analysis.

The first EOF mode of summer OLR (Fig. 1a) accounts for about 12% of the total variance. The most conspicuous feature of this mode is a seesaw in convection between the EEIO and the western Pacific with the node point over the Maritime Continent (Zhu and Wang 1993). The second EOF mode (Fig. 1b) explains 8.4% of the total variance. This mode describes a connection of convection between the Indian subcontinent and Maritime Continent; meanwhile, opposite convection phase is evidenced over the south equatorial Indian Ocean and western Pacific. The third EOF mode displays the variation centers over the western Pacific Ocean (figure not shown), therefore it will not be discussed in detail. The spatial patterns of the first two EOF modes agree well with previous results (e.g., Lau and Chan 1986; Lawrence and Webster 2001). As already illustrated by these studies, these two modes in fact reflect the same propagating BSISO mode at different propagating phases (e.g., Waliser et al. 2003). Figure 1c shows the lag–correlation coefficients between the two leading EOF modes. The maximum lagging/leading correlation occurs around the negative/

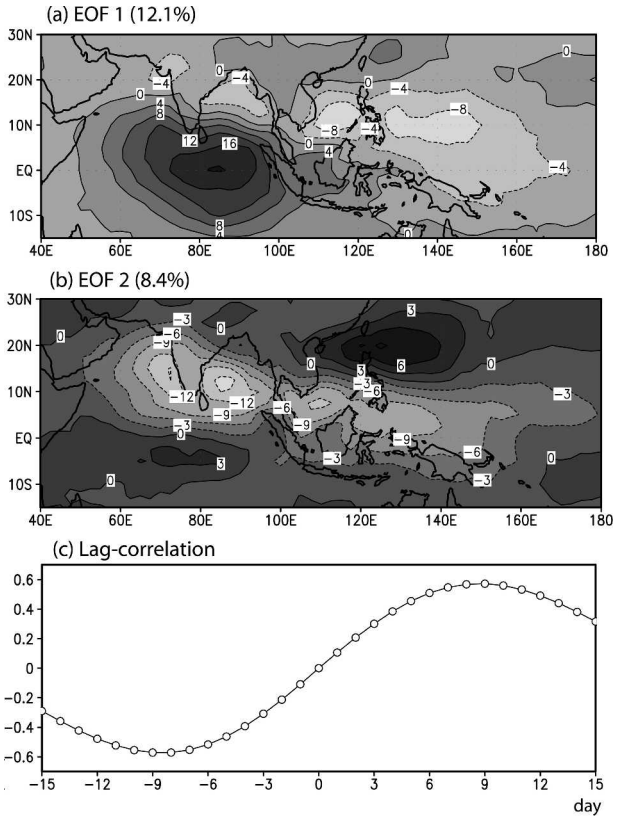

FIG. 1. (a) First and (b) second EOF modes of summer OLR and (c) the lag–correlation between the time series of these two modes. The two EOF modes have been scaled by one std dev of the time series to give a unit of W m^{-2}; they occupy 12.1% and 8.4% of the total variance, respectively. Positive coefficients in (c) represent that the second EOF mode leads the first one.

positive ninth day, implying a period of around 35 days for the BSISO.

Next, the time series of the first EOF mode is used to select strong ISO events for the composite. Here the strong ISO events are identified by the time series exceeding one standard deviation, as indicated by the two horizontal dashed lines in Fig. 2. For very few cases with multiple extremes within a very short time (10 days), only one peak is selected by a subjective inspection of the OLR evolution pattern. During the 22-yr period, there are 59 cases with a positive OLR phase (suppressed convection over the EEIO according to the EOF1) and 67 cases with a negative OLR phase (enhanced convection over the EEIO), with an average of 3 enhanced and 3 suppressed convection cases each year. Then, composite evolution fields for the OLR (as well as other variables) are obtained by averaging over all selected ISO events with respect to the day corresponding to each peak (negative or positive) in the time series of the first EOF mode; this day is designated as composite day 0. Note that while the reference time (i.e., day 0) is determined based on the EOF1 time series, the actual data used for the composite were from the 20–70-day-filtered data. The composites are first constructed independently for both positive and negative OLR phases. The composite results for the positive and negative OLR phases display a rather mirror image with an opposite sign. Thus, a negative-minus-positive OLR phase composite is further conducted, which reflects the case with enhanced ISO convection over the EEIO.

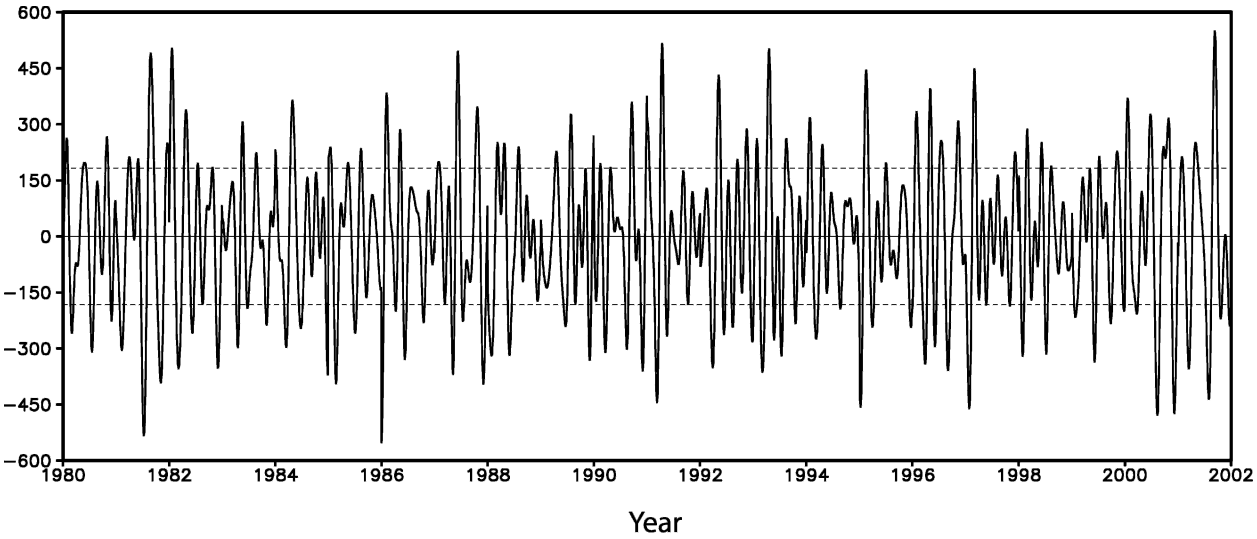

FIG. 2. Time series of the first EOF mode of the OLR in Fig. 1 during the 22-yr period. The two horizontal dashed lines represent positive/negative one std dev.

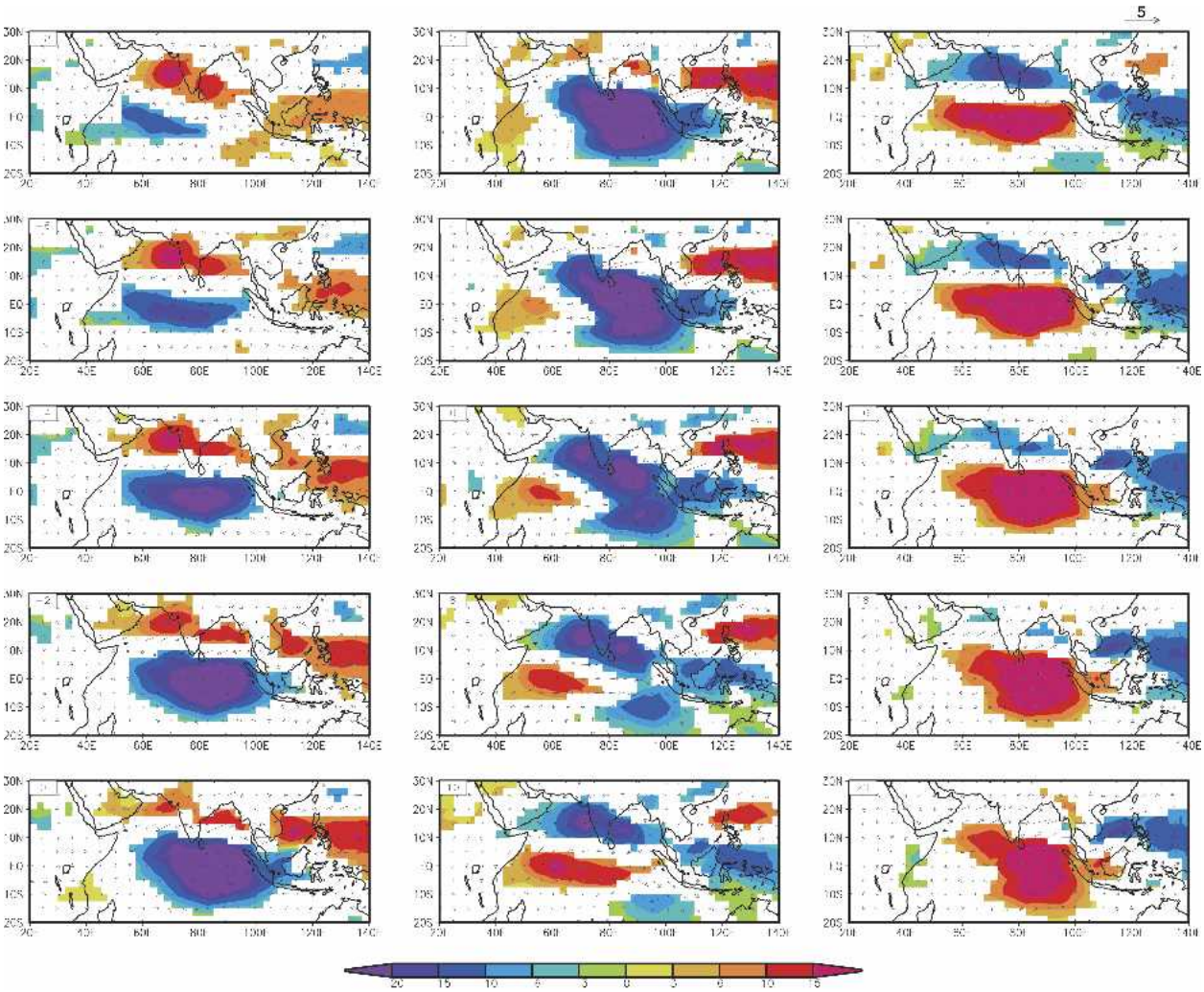

FIG. 3. Evolution of the composite OLR perturbation (W m^{-2}) and 925-mb wind (m s^{-1}) fields from day −8 to day 20 with an interval of 2 days. The negative OLR represents convection. Day 0 is a reference time corresponding to the peaks in the time series of the first EOF mode for each selected strong ISO case.

Figure 3 shows the composite evolution of OLR (shading) and 925-mb winds (arrows) from day −8 to day 20 with an interval of 2 days, in which the OLR field is only plotted in the regions where the difference over the means is statistically significant at the 95% confidence level by the two-sample *t* test. Note that the composite OLR pattern at day 0 greatly resembles the first EOF mode (Fig. 1a) with an opposite sign, whereas the composite OLR pattern at day 8 resembles the second EOF mode (Fig. 1b), which provides further support for the previous discussion that the two leading EOF modes represent the same BSISO mode at different phases.

As shown by Fig. 3, at day –8, the convection is located over the WEIO and is relatively weak. In the ensuing days, it keeps moving eastward along the equator toward the EEIO and intensifies. After the convection center arrives at around 90°E, it tends to be stationary in space (e.g., after day –2), then keeps intensifying locally and begins to expand meridionally. Around this moment (day 0), it is noticed that suppressed convection emerges over the WEIO off the eastern African coast. After that, this suppressed convection intensifies very quickly and shifts eastward along the equator. After it arrives at the EEIO around 90°E, an enhanced convection tends to emerge over the WEIO (e.g., after day 18), exhibiting a very similar behavior with the previous opposite cycle. Then another BSISO cycle begins; so on and so forth, the oscillation continues.

On the other hand, as also shown by Fig. 3, during the early developing stage of convection over the equato-

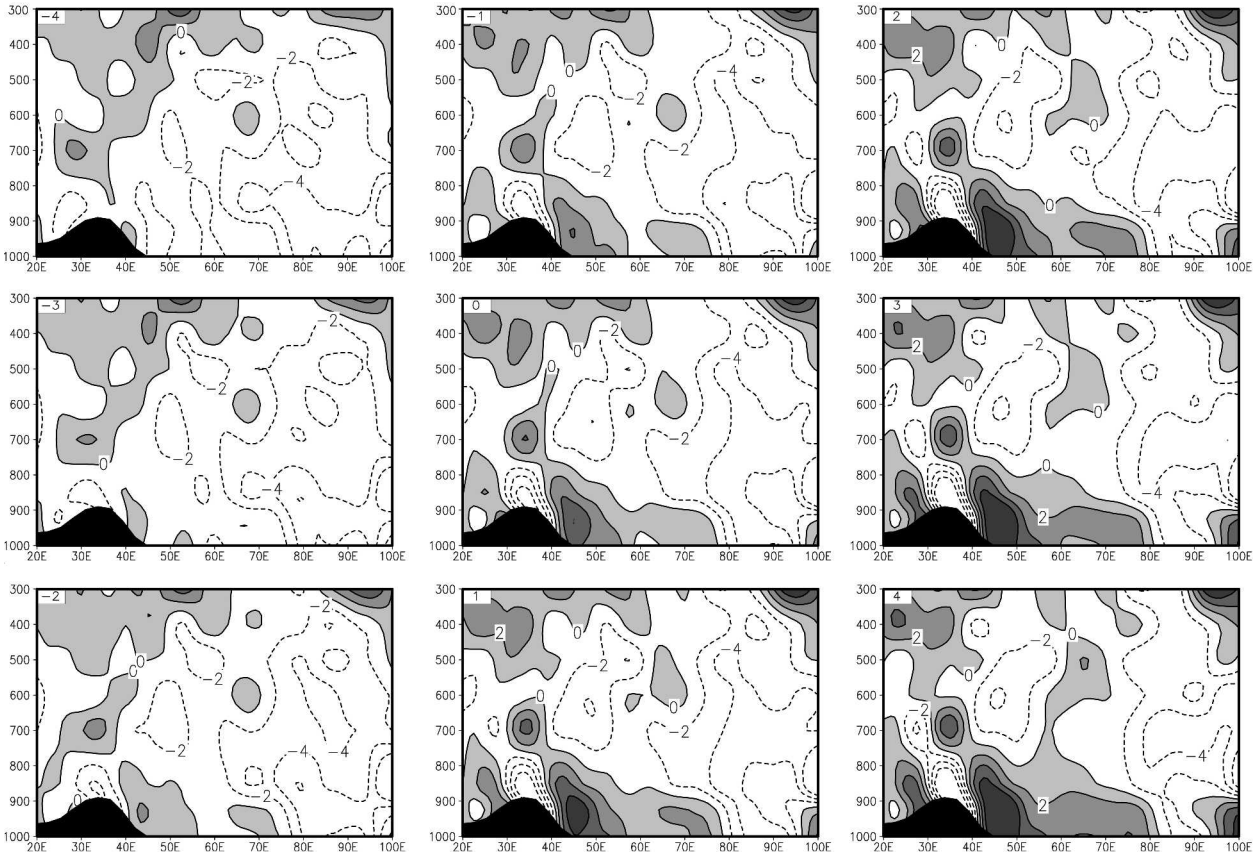

FIG. 4. Evolution of longitudinal–vertical profile of perturbation divergence fields (10^{-7} s^{-1}) by composite analysis. The fields are averaged over the latitudes 5°S–2.5°N. The vertical axis is height by pressure (unit: hPa). The regions with divergence are shaded. The dark shading in the lower-left corner of each panel shows the topography over eastern Africa, which is also averaged over the latitudes 5°S–2.5°N.

rial Indian Ocean (e.g., day –6), the low-level wind perturbation is very weak and less well organized along the equator. With the development of the convection in the following days, the wind circulation gradually enhances and becomes well established, with westerlies to the west of and within the convection center and two cyclonic gyres over both sides off the equator, exhibiting a main feature depicted by a Gill-type solution (Gill 1980), which suggests that the ISO convective heating could be responsible for this low-level wind pattern. Additionally, northward-crossing equatorial wind over the WEIO is evidenced accompanying the reinitiation of suppressed convection in situ. A similar feature in the wind fields can also be found during the following opposite cycle (e.g., after day 12).

To achieve a better understanding of this BSISO oscillating behavior, in this study we will devote our efforts to explaining how the new enhanced/suppressed convection is reinitiated over the WEIO after its previous opposite cycle propagates into the EEIO. Since the positive and negative OLR phase composites largely mirror each other, our description and discussion will focus on the reinitiation process of the suppressed convection over the WEIO in the presence of enhanced convection over the EEIO (e.g., day 0 in Fig. 3) in the following context.

To illustrate the physical processes associated with the BSISO reinitiation process, the divergence field during the reinitiation period is examined based on a similar composite analysis. Figure 4 presents the evolution of the divergence field with a longitudinal–vertical cross section averaged between 5°S and 2.5°N around day 0. The topography of eastern Africa (also averaged between 5°S and 2.5°N) is marked by the dark shading in each panel. It shows that about 2 days prior to the reinitiation of suppressed convection over the WEIO (e.g., day –2), a local divergence perturbation becomes visible in the boundary layer in situ (40°–60°E). After that, this divergence perturbation intensifies rapidly and extends eastward. Consistent with the evolution of

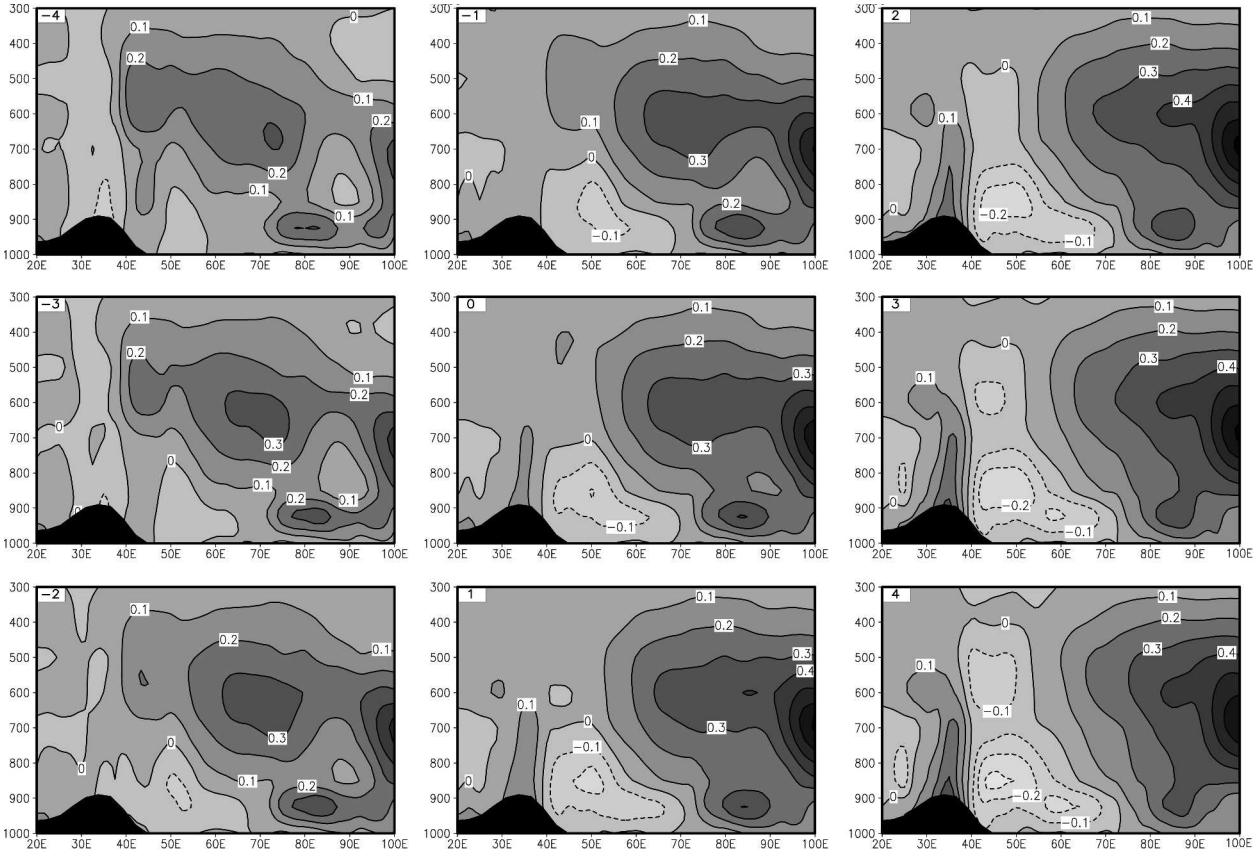

FIG. 5. Same as in Fig. 4, except for perturbation specific humidity field (g kg^{-1}).

this PBL divergence field, downward motion in the lower troposphere is observed during the reinitiation process (figure not shown). Meanwhile, a reduced specific humidity center is also detected in the lower troposphere during the reinitiation of suppressed convection in situ (Fig. 5). Similar to the divergence field, this reduced specific humidity perturbation first emerges in the PBL around 2 days prior to the reinitiation, then quickly intensifies and extends up to 400 mb. The cooccurrence of both the reduced specific humidity and low-level divergence suggests that the reinitiation process of suppressed convection could be caused by the reduction of the PBL moisture associated with the boundary layer divergence.

Another intriguing fact that one may notice is that the low-level perturbation divergence field over the WEIO and eastern Africa displays a three-cell wave pattern (see Fig. 4; more obvious after day –1), with a positive center (divergence) over the WEIO, a negative cell over coastal Africa, and another positive one to the farther west. These three divergence cells are established along the reinitiation phase of the suppressed convection over the WEIO. After that, they become stationary spatially and intensify. This three-cell wave pattern in the divergence field is mainly confined in the boundary layer.

Figures 6a and 6b present the horizontal patterns of the low-level divergence (850 mb) and specific humidity (925 mb) perturbation fields, which are taken from composite day 0. This three-cell divergence pattern over the WEIO and eastern Africa as noted above can be clearly evidenced in Fig. 6a. The divergence center over the WEIO off the African coast is rather consistent with the positive OLR anomaly in situ by Fig. 3 (day 0), indicating the reinitiation of suppressed convection. Additionally, the horizontal pattern of this positive perturbation divergence over the western Indian Ocean between 40° and 70°E also corresponds very well to the local reduced specific humidity as shown by Fig. 6b. Further inspection of the surface latent heat flux at this moment, however, shows a positive center over this region (Fig. 6d), which suggests that the reduction of specific humidity in the PBL during the reinitiation process is not due to the surface evapora-

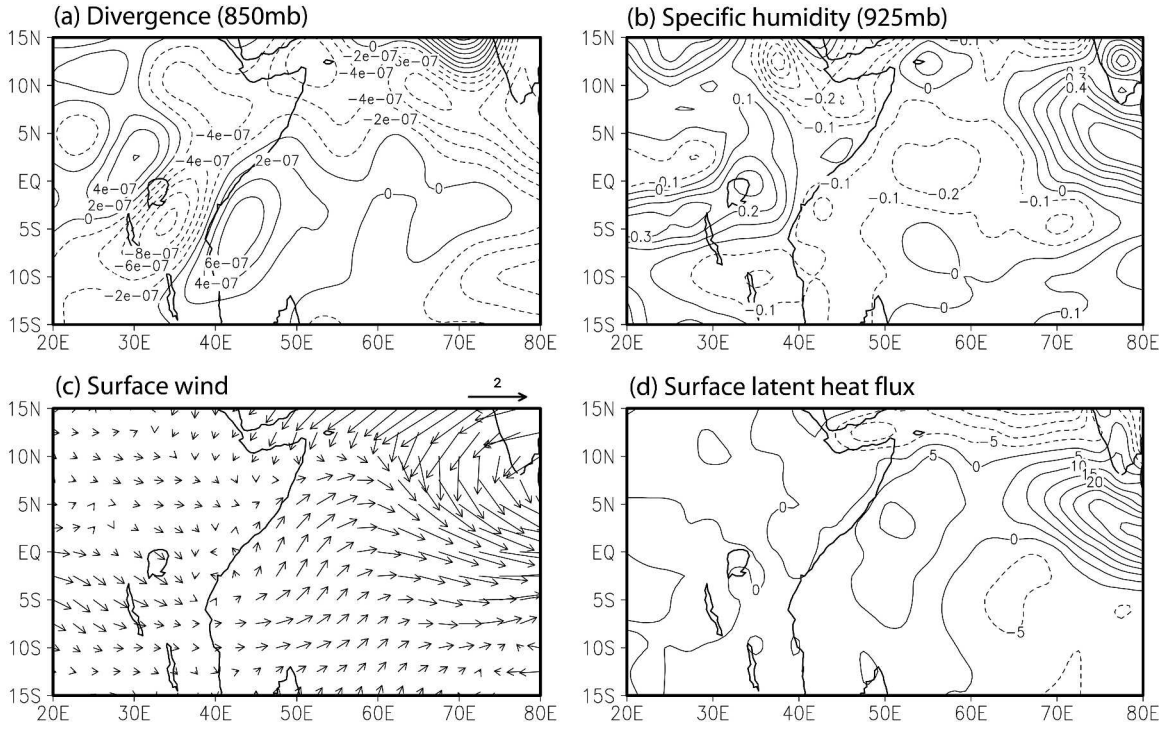

FIG. 6. (a) 850-mb divergence (s^{-1}), (b) 925-mb specific humidity (g kg^{-1}), (c) surface wind (m s^{-1}), and (d) surface latent heat flux (W m^{-2}) at composite day 0 based on the NCEP–NCAR reanalysis. All variables shown are the perturbation fields.

tion. That is to say, the PBL divergence could play a role for this reduction of moisture during the reinitiation period. This enhanced surface latent heat flux over the WEIO off the African coast in Fig. 6d could be explained by the perturbation surface wind in situ as displayed by Fig. 6c, as the southwesterly perturbation wind enhances the mean northward cross-equatorial flow, thus increasing surface evaporation.

Both the vertical (Fig. 4) and horizontal (Fig. 6a) structures of the three-cell wave pattern of the perturbation divergence field bear an intimate relationship with the topography over eastern Africa (Fig. 7).

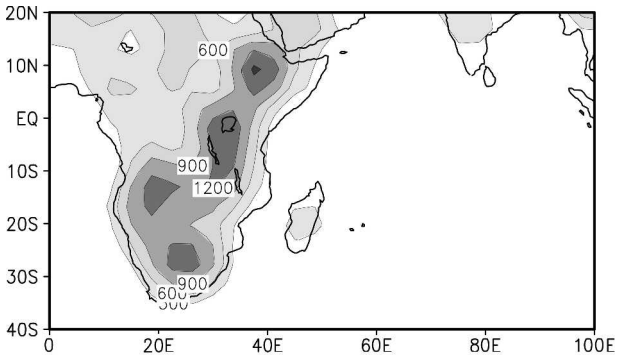

FIG. 7. Topography of the African continent (m).

Therefore, questions are raised: What is the role of the topography over the eastern Africa for the reinitiation of suppressed convection? Is the topographic effect essential for this reinitiation process or are other important factors involved? In the next section, we intend to investigate the physical mechanisms responsible for the establishment of the PBL divergence pattern over the WEIO, which could be the triggering factor for the reinitiation of the suppressed convection as illustrated by the previous results.

4. The BSISO reinitiation mechanism

In this section, we rely on an anomalous run in an AGCM to reveal the physical mechanisms involved in this ISO reinitiation process over the WEIO. Our strategy is to illustrate how the low-level perturbation divergence is generated over the WEIO off the African coast in the presence of a prescribed diabatic heating over the EEIO, a scenario depicted in Fig. 3 at day 0. The details of the model employed here have been discussed in section 2.

The diabatic heating over the EEIO prescribed in the AGCM is based on the OLR pattern during the reinitiation phase (e.g., day 0 in Fig. 3). The horizontal pattern of the heating is displayed in Fig. 8a, with the

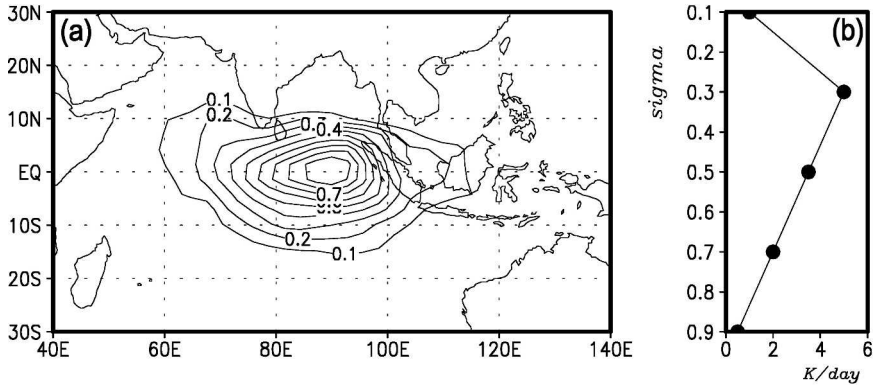

FIG. 8. (a) Horizontal distribution and (b) vertical profile of the diabatic heating (K day^{-1}) prescribed in the AGCM. The pattern in (a) is adopted from the negative OLR (convection) distribution over the EEIO at composite day 0 in Fig. 3. The vertical coordinate in (b) represents sigma levels in the model.

maximum center located around 90°E at the equator. The vertical heating profile is given in Fig. 8b, with the maximum heating rate at $\sigma = 0.3$ (about 300 mb) with 5 K day^{-1}. This vertical profile is adopted based on the vertical structure of vertical velocity for the ISO convection as indicated by previous results (e.g., Jiang et al. 2004) and is consistent with other studies (e.g., Annamalai and Sperber 2005). This model is integrated for 20 days to obtain an equilibrium state in response.

First we examine the simplest case, a resting environmental flow case. Figure 9a displays the longitudinal–vertical profile of the perturbation zonal wind along the equator. The result shows that in response to the prescribed convective heating, an easterly wind perturbation appears to the east of the heat source and westerly wind to the west in the lower troposphere. At the upper levels, the circulation tends to reverse. This baroclinic structure of perturbation wind induced by the diabatic heating bears close similarity with the classical Gill-type solution.

In the second experiment in which a realistic 3D summer mean state is specified, an east–west asymmetry of the wind circulation is clearly visible about the heating center as shown in Fig. 9b. To the east of the heating center, the zonal wind exhibits a baroclinic structure, similar to the resting environmental flow case in Fig. 9a.

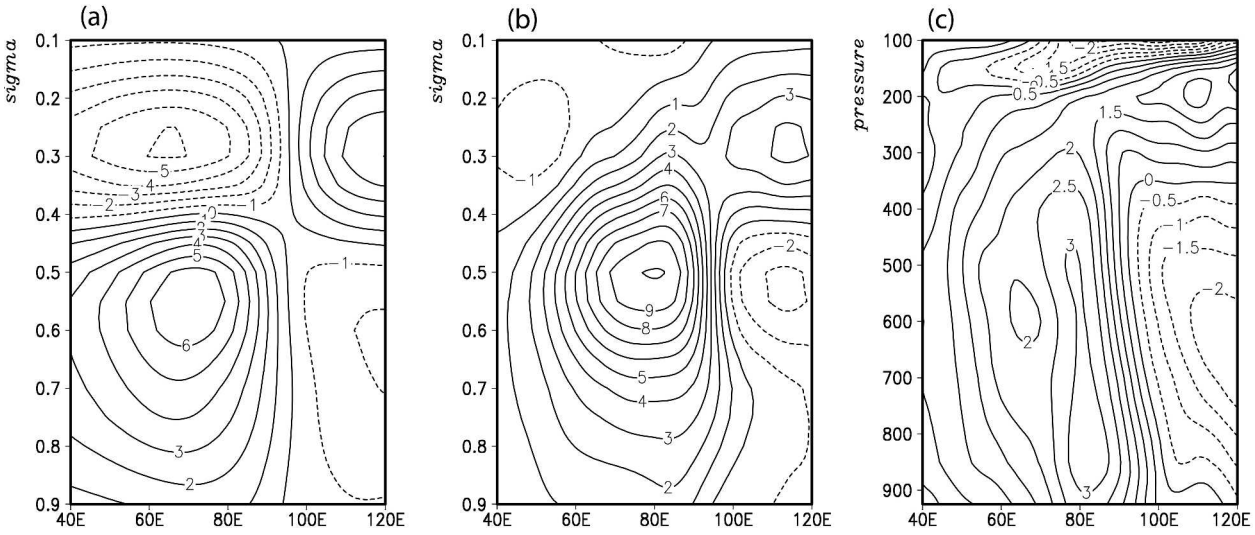

FIG. 9. Longitudinal–vertical profile of wind u component (m s^{-1}) along the equator: (a) by AGCM experiment with a resting environmental flow, (b) by the experiment with summer mean flow, and (c) by NCEP–NCAR reanalysis at composite day 0. The vertical coordinates for (a) and (b) are the sigma levels in the model, and the vertical coordinate for (c) is pressure (hPa).

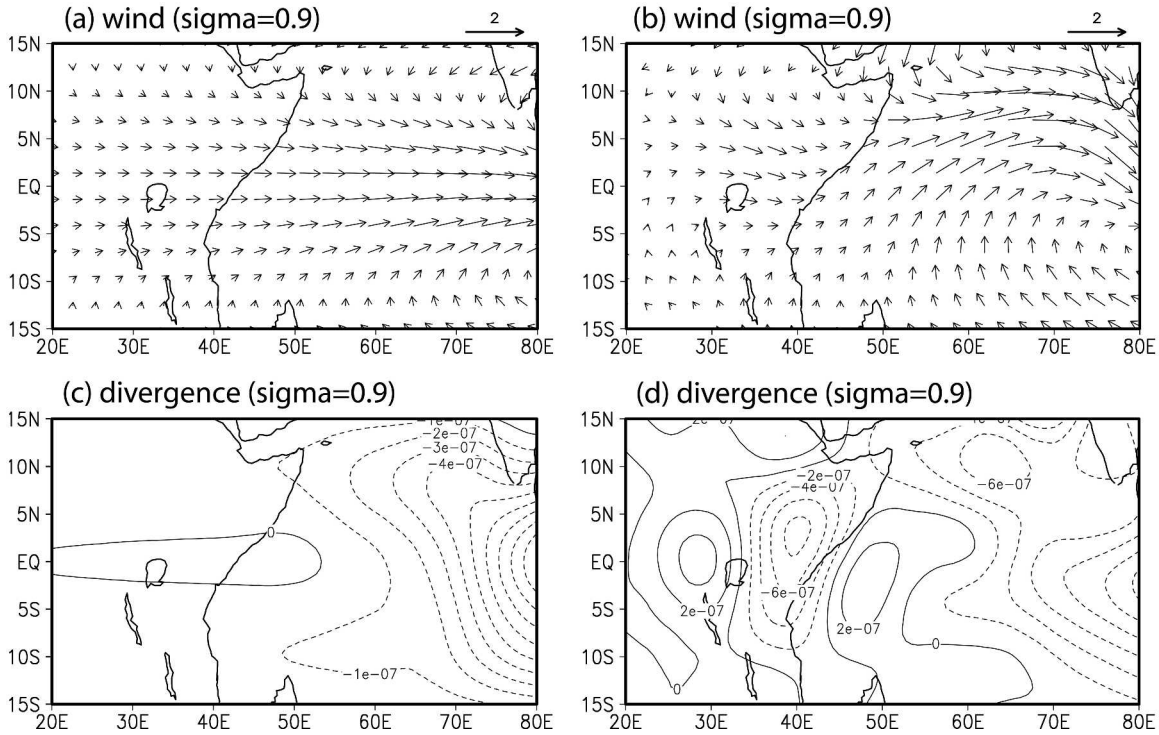

FIG. 10. Perturbation wind field (m s^{-1}) (a) by the experiment with a resting environmental flow and (b) by the experiment with summer mean state; and perturbation divergence fields (s^{-1}) (c) by the experiment with a resting environmental flow and (d) by the experiment with summer mean state. All the fields are from the $\sigma = 0.9$ level.

However, in contrast to the previous case, the *u*-wind bears an equivalent barotropic structure west of the heating with westerlies from the lower to upper troposphere. This asymmetry of zonal wind response is also present in the observed composite (Fig. 9c). The diagnosis for the momentum equation reveals that the vertical advection of the momentum u-component by both the mean and perturbation vertical velocity plays an essential role for this equivalent barotropic structure to the west of the heat source (figure not shown).

The horizontal pattern of the low-level ($\sigma = 0.9$) perturbation wind fields simulated by these two experiments is further illustrated by Figs. 10a and 10b. For the resting environmental flow case, the low-level wind pattern over the WEIO and Africa displays a westerly along the equator with cyclonic circulation off both sides of the equator (Fig. 10a), representing the two Rossby gyres as described by the classical Gill solution. In the presence of summer mean flow, however, the low-level perturbation wind fields over the WEIO exhibit a strong northward cross-equatorial flow (Fig. 10b), very close to the observations (see Fig. 6c). Obviously, the summer mean flow plays an important role for this observed northward cross-equatorial flow.

The purpose of this study is to explain the BSISO reinitiation process over the WEIO, or more specifically, to understand how the low-level divergence is generated during the reinitiation. To this end, the divergence fields simulated by the aforementioned two experiments at the $\sigma = 0.9$ level are examined. Figure 10c illustrates the low-level divergence field in the experiment with a resting environmental flow. It shows that in response to the heat source over the EEIO, a low-level divergence perturbation is generated over the WEIO and Africa. This divergence is ascribed to the decrease of westerly wind to the west along the equator, which is a part of the Rossby wave response to the diabatic heating over the EEIO as also discussed by Matthews (2000). However, the magnitude of the divergence field in this case is one order of magnitude smaller than the observed (see Fig. 6a). Figure 10d displays the divergence field in the summer mean flow case. Note that the observed three-cell divergence pattern is well captured by this simulation, with a positive cell over the western Indian Ocean, a negative center along the African coast (between 30° and 40°E), and another positive center farther to the west. The location of the three cells shows a good coincidence with the

orography in eastern Africa as shown in the observation. It is also worth noting that the magnitude of the divergence maximum over the WEIO is in the same order as the observed, although slightly weaker. Based on the results above, we conclude that the weakening of the Rossby wave response to the west of the heat source may not play a fundamental role for reinitiation of the BSISO.

Next, we intend to investigate the relative role that the mean flow and topography play in causing the divergence field over the WEIO. Strictly speaking, the mean flow and the topographic effects are inseparable; for instance, the Somali Jet is related to the African topography. For the purpose of elucidation, in the following we intentionally remove the topographic effects over eastern Africa by replacing the mean surface pressure and temperature specified in the model over the African continent from the southern tip to 20°N with their corresponding zonal mean values at each level, while keeping the observed 3D mean flow pattern. This experiment is defined as experiment "EXP_NOTP." Figure 11a shows the divergence field at the $\sigma = 0.9$ level in this experiment. Despite the unclear three-cell wave pattern in this experiment compared with the full mean state case (Fig. 10d), the divergence center over the WEIO still exists, and its amplitude is slightly reduced. This result suggests that the eastern African mountains may play an important role for the two cells of the divergence field over the continent, while the divergence in the WEIO could be primarily determined by the interaction between the ISO circulation and summer basic state. On the other hand, the topographic effect may enhance the intensity of this divergence perturbation over the WEIO. Hence, a key question we intend to address next is how the asymmetric 3D mean flow modulates the atmospheric response to the ISO heating in the EEIO and leads to a PBL divergence over the WEIO.

To extract the essential process that gives rise to the low-level divergence over the WEIO, we examine the role of each term in momentum and thermodynamic equations of the model by switching it on or off based on the EXP_NOTP run. It turns out that the temperature advection terms are crucial in generating the PBL divergence. Figure 11b provides the divergence field at $\sigma = 0.9$ when the temperature advection terms (including both the vertical and horizontal advection terms) are turned off. In this case, the amplitude of divergence over the WEIO is reduced by an order of magnitude.

To understand how the temperature advection affects the generation of divergence over the BSISO reinitiation region, a diagnosis for the total temperature advection term is conducted. The result indicates that the horizontal temperature advection term dominates the total contribution (figure not shown). Also, it is noted that the vertical temperature advection term is always offset by the adiabatic term; and usually it is the combination of these two terms that represents the real adiabatic effect, which can be physically interpreted by the vertical advection of potential temperature. Figure 11c illustrates the horizontal temperature advection

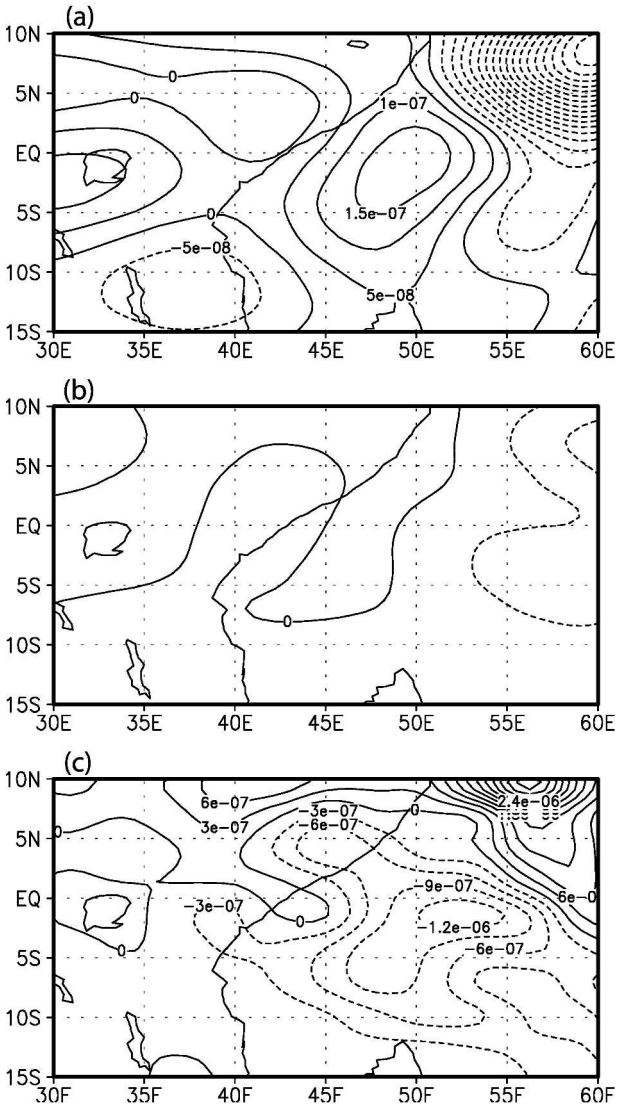

FIG. 11. Distribution of perturbation divergence (s^{-1}) at the $\sigma = 0.9$ level (a) in the experiment EXP_NOTP and (b) in the experiment based on the EXP_NOTP run with the temperature advection terms shut off. (c) Distribution of horizontal temperature advection at $\sigma = 0.9$ in the experiment EXP_NOTP (K day^{-1}). The intervals of the contours in both (a) and (b) are 0.55×10^{-8} s^{-1}.

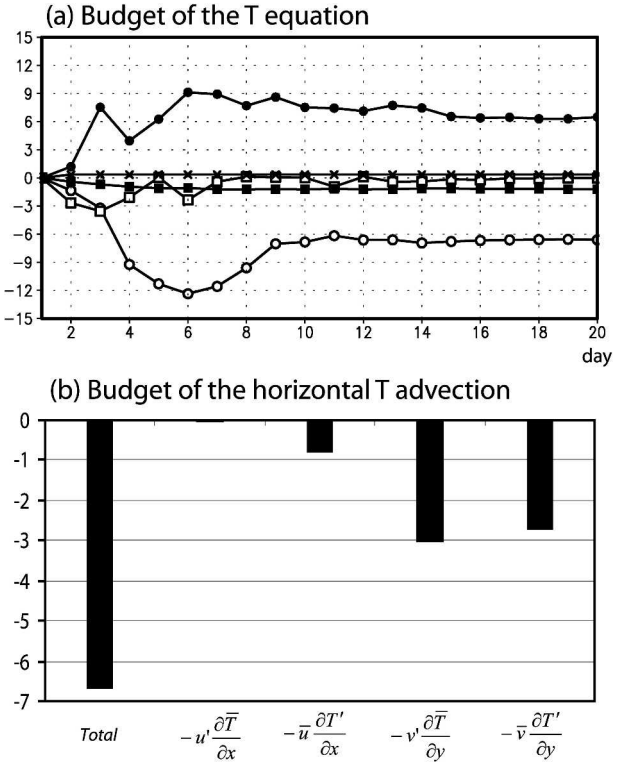

FIG. 12. (a) Evolution of each term in the temperature Eq. (A2) during the model integration based on the EXP_NOTP run: $-\mathbf{V}\cdot\nabla T$ (open circles), $\dot{\sigma}[(kT/\sigma) - (\partial T/\partial\sigma)]$ (solid circles), $kT(\mathbf{V} - \tilde{\mathbf{V}})\cdot\nabla \ln P_s$ (solid squares), $-kT\tilde{D}$ (open squares), and $(\dot{Q}/C_p)$ (crosses). All the terms shown are perturbation terms. (b) Contributions for the total horizontal temperature advection, which is calculated from the equilibrium state at model day 20. Each term in both (a) and (b) is averaged over the region 10°S–5°N, 45°–55°E at the $\sigma = 0.9$ level with a unit of 10^{-7} K $\times$ s^{-1}.

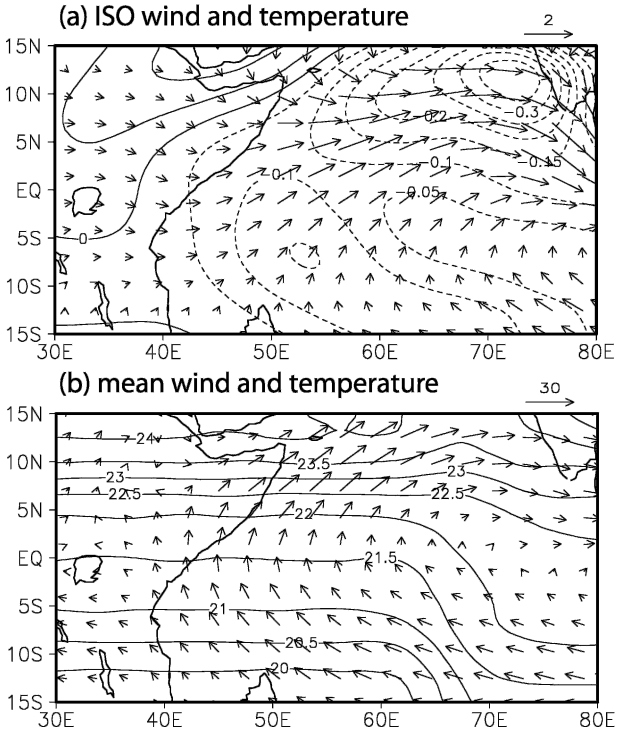

FIG. 13. (a) ISO perturbation wind (m s^{-1}) and perturbation temperature (K); (b) summer mean flow (m s^{-1}) and mean temperature (°C). All fields are from the $\sigma = 0.9$ level in the EXP_NOTP experiment.

pattern at the model level $\sigma = 0.9$ in the EXP_NOTP run. Compared to the corresponding divergence field in Fig. 11a, it is noted that a cold temperature advection center over the WEIO coincides well with the divergence center. Then a diagnosis of the heat budget based on the temperature equation is carried out in order to reveal the physical linkage between the cold temperature advection and divergence fields. Figure 12a presents the evolution of main terms in the temperature equation [see Eq. (A2) in the appendix] at the $\sigma = 0.9$ level during the 20-day integration period in the EXP_NOTP run. All of these terms are taken averaged over the region between 10°S and 5°N, 45° and 55°E, where the cold temperature advection and divergence centers are mainly located. As shown in Fig. 12a, the most dominant terms contributing to the temperature tendency are the horizontal temperature advection term $[(-\mathbf{V}\cdot\nabla T)']$; open circles] and the adiabatic process ($\{\dot{\sigma}[(kT/\sigma) - (\partial T/\partial\sigma)]\}'$; solid circles). {Note that further calculation shows that most of the contribution to this adiabatic term results from $\dot{\sigma}'[(k\bar{T}/\sigma) - (\partial\bar{T}/\partial\sigma)]$}. The amplitudes of the other terms including the diabatic heating are negligible during this initial development phase. Namely, the cold horizontal temperature advection in the PBL is offset by the adiabatic warming process through an induced downward motion. This downward motion is further associated with the low-level divergence due to the mass continuity.

To detect the principal processes responsible for the cold horizontal temperature advection over the WEIO, we conduct a budget analysis for each horizontal temperature advection term (Fig. 12b). The result points out two major terms, that is, the meridional temperature advection of mean gradient by ISO wind and the perturbation gradient by the mean flow. These two terms have comparable magnitudes. The zonal advection terms, on the other hand, are negligible compared to their meridional counterparts.

Figure 13 shows the ISO perturbation wind and temperature fields as well as the basic-state wind and temperature fields at the model level $\sigma = 0.9$ in the EXP_NOTP run. Note that the low-level ISO pertur-

bation wind in this experiment (Fig. 13a) exhibits an obvious northward cross-equatorial component over the WEIO, as in the experiment with full summer mean state (Fig. 10b) and observations (Fig. 6c), in contrast to the result of the resting environmental flow case (Fig. 10a). It suggests that the asymmetric wind response over the WEIO is a result of the effect by the 3D summer mean flow.

How does the mean flow modulate the Gill solution, leading to an asymmetric response? Our idealized numerical experiments with a zonal mean basic state[1] show that this low-level cross-equatorial perturbation flow is primarily caused by the asymmetry (relative to the equator) of the easterly vertical shear of the mean flow. The analytical study by Wang and Xie (1996) indicates that Rossby wave responses are amplified in the lower troposphere in the presence of easterly vertical shear, and vice versa. During boreal summer, the strong easterly vertical shear is confined to the north of the equator over the south Asian monsoon region. As a result, the low-level Rossby gyres induced by the diabatic heating over the EEIO exhibit an asymmetry about the equator with a much stronger northern branch and a weaker one to the south. This leads to a meridional pressure gradient and a northward cross-equatorial perturbation flow. In addition, the strong horizontal shear of low-level zonal mean flow, with westerlies to the north of equator and easterlies to the south, could also lead to an asymmetry in the Rossby wave responses, as illustrated by Wang (2000) that the westerly/easterly mean flow tends to enhance/suppress Rossby wave responses. The northward cross-equatorial perturbation wind induced by the vertical and horizontal shear of the mean flow can be further enhanced through the advection by the strong mean meridional flow in the lower troposphere (Somali Jet).

On the other hand, the summer mean temperature in the low level also exhibits a strong asymmetry (Fig. 13b). The maximum mean temperature over the western Indian Ocean is observed around 13°N. As a result, the advection of the cold mean temperature by the northward cross-equatorial perturbation wind $[-v'(\partial\overline{T}/\partial y)]$ tends to generate a cold temperature center over the WEIO.

Meanwhile, the perturbation temperature field (Fig. 13a) also shows a clear asymmetry about the equator in the western Indian Ocean (around 50°E). It is anticipated that this asymmetric perturbation temperature field advected by the strong northward cross-equatorial basic flow $[-\overline{v}(\partial T'/\partial y)]$ would also give rise to a cold temperature advection over the WEIO. This process has a comparable magnitude with that by the ISO perturbation flow $[-v'(\partial\overline{T}/\partial y)]$ as shown in Fig. 12b. Then, in order to gain some clues on the physical causes responsible for this perturbation temperature asymmetry over the western Indian Ocean, we analyze the result from the resting environmental experiment run, in which case the perturbation temperature field shows two negative centers in the WEIO, symmetric about the equator (figure not shown). The diagnosis shows that these two cold perturbation temperature centers are closely linked to the adiabatic cooling due to upward motion in the two Rossby gyres in the absence of the diabatic heating. With the inclusion of the summer mean flow in the experiment EXP_NOTP, the perturbation temperature in the PBL is greatly modulated by the temperature advection terms, and as a result it becomes asymmetric about the equator as shown in Fig. 13a.

To sum up, the results based on numerical study presented in this section have demonstrated that in the presence of the 3D summer mean state, to respond a convective heating over the EEIO, a PBL divergence perturbation could be induced over the WEIO, which is found to be associated with the reinitiation of suppressed convection in situ. Diagnosis illustrates that the low-level cold horizontal temperature advection over the WEIO plays an essential role for this PBL divergence. Two meridional temperature advection terms are most important for the total horizontal temperature advection and result from the interaction between the 3D summer mean state and the asymmetric atmospheric circulation induced by the ISO convective heating over the EEIO.

It's worthwhile to mention that the mechanism responsible for the reinitiation of suppressed convection over the WEIO described above could also be applicable for its opposite phase, that is, the reinitiation of an enhanced convection over the WEIO in the presence of a strong suppressed ISO convection over the EEIO (a scenario by day 18 in Fig. 3). By specifying a diabatic cooling over the EEIO, with the same horizontal and vertical structures as for the diabatic heating previously described, a low-level convergence perturbation center can also be detected over the WEIO by the AGCM simulation, indicating a linear behavior during this process.

5. Verification with the NCEP–NCAR reanalysis

The physical processes illustrated above for the BSISO reinitiation are based on the model simulation.

[1] This zonal mean basic state is based on the observed 3D basic state averaged between 40° and 120°E.

One may notice that the AGCM has been integrated for 20 days to obtain an equilibrium state of the atmospheric response to the diabatic heating/cooling in the previous model simulation (in fact, after the integration for 8 days, this equilibrium state is almost achieved, as shown in Fig. 12a), facilitating a contrast to the period of 35 days with the observed BSISO. It is worth noting that this time duration for reaching the steady state is largely controlled by the Rayleigh friction and Newtonian cooling coefficients set in the model, which have an *e*-folding time scale of 10 days in the current AGCM. By selecting this parameter, we can clearly demonstrate the adjustment processes involved during the reinitiation period over the WEIO. In the reality, however, this adjustment process for the atmospheric response to the diabatic heating/cooling could be accomplished very shortly. Also it is possible that the complete equilibrium state could not be reached during the evolution of the BSISO, while the interactive heating involved in the reality could also play an important role for the rapid amplification of the convection perturbation after its reinitiation, which is not represented by the current AGCM. Based on these considerations, we believe that our understandings for the BSISO reinitiation over the WEIO obtained based on previous numerical studies could provide us a new vision for the observed BSISO. In this section, we intend to verify these important features obtained by the AGCM simulation with the NCEP–NCAR reanalysis.

Figure 14a shows the horizontal temperature advection field at 925 mb at composite day 0 by the reanalysis. As mentioned in the previous sections, at this time the main convection is located in the EEIO, and reinitiation of suppressed convection is perceived over the WEIO (Fig. 3). Consistently, a divergence field precedes the suppressed convection by a few days (Fig. 4). Of particular interest, as illustrated in Fig. 14a, is the collocation of the divergence field (Fig. 6a) and cold horizontal temperature advection over the BSISO reinitiation region (Fig. 14a), closely resembling the results by the model simulation (e.g., Fig. 11). This most essential feature during the BSISO reinitiation process as illustrated by the numerical study is confirmed by the observations; that is, the cold horizontal temperature advection might play an essential role in the generation of the divergence field in the real world.

To further evaluate this point, the temporal phase relationship between the horizontal and vertical temperature advection and divergence at 925 mb over the reinitiation region (10°S–5°N, 40°–60°E) is explored based on the reanalysis data (Fig. 14b), where each variable is normalized by its corresponding maximum magnitude. The result displays an out-of-phase relationship between the perturbation vertical temperature advection and divergence fields, as one would expect based on the continuity equation.[2] More interestingly, the horizontal temperature advection over the WEIO tends to precede both the vertical temperature advection and divergence fields by about 2 days. For instance, at day −4 the horizontal temperature advection at 925 mb tends to transit from a positive to negative phase over the BSISO reinitiation region; and two days later (day −2), the divergence field begins to change phase. This observed fact provides further evidence that the cold horizontal temperature advection in the lower troposphere over the WEIO could be essential for the divergence field in situ, which could be responsible for the reinitiation of a suppressed convection phase in the BSISO cycle.

The relative importance of various temperature horizontal advection terms over the reinitiation region is further examined based on the reanalysis data. Consistent with the AGCM results, the total horizontal temperature advection is primarily contributed by two meridional advection terms (figure not shown). All of these results imply that the AGCM simulation captures the principal features of the observed BSISO during its reinitiation phase over the WEIO, and the proposed mechanism for the BSISO reinitiation based on the AGCM simulation may shed light on understanding the real world.

6. Summary and discussion

The goal of this study is to reveal the observed characteristics of the BSISO during its reinitiation phase and to understand the physical mechanism responsible for this reinitiation process. For this purpose, a composite analysis is first conducted based on the time series of the leading principle components of the OLR during 1980–2001.

The composite results demonstrate that the reinitiation of a new convection phase of the BSISO cycle tends to take place over the WEIO near the coast of eastern Africa after the previous opposite convection cycle propagates into the EEIO around 90°E. Considering that the composite features for the positive and negative BSISO cycles largely mirror each other, our

[2] Diagnosis indicates that the contribution by the term $-\overline{w}(\partial T'/\partial p)$ is much less than that by $-w'(\partial \overline{T}/\partial p)$ for the total vertical temperature advection, which is also pointed out by the model simulation.

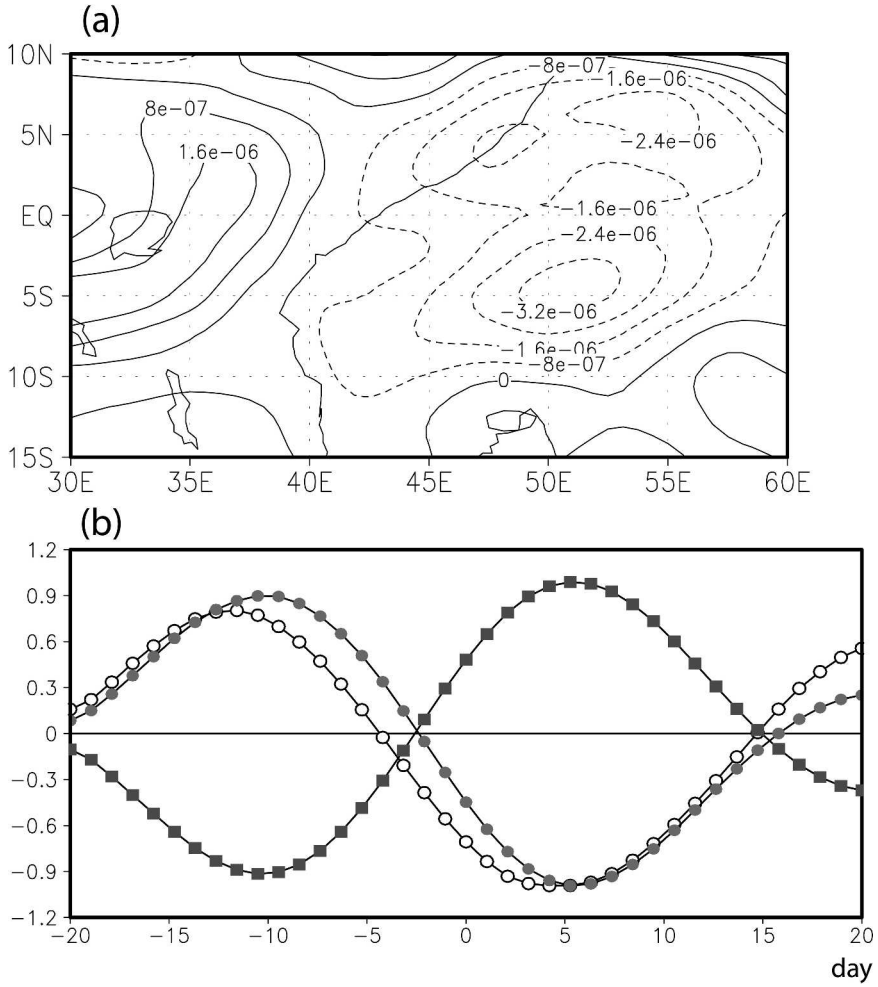

FIG. 14. (a) Distribution of horizontal temperature advection (K s^{-1}) at composite day 0; (b) evolution of the horizontal (open circles) and vertical temperature advection (solid circles) and divergence field (solid squares) over the BSISO reinitiation region, 10°S–5°N, 40°–60°E, where each term is standardized by its corresponding maximum amplitude. All variables in both (a) and (b) are based on the composite results with the NCEP–NCAR reanalysis at the 925-mb level.

discussion is mainly focused on the reinitiation of suppressed convection over the WEIO while there is enhanced convection over the EEIO. It's illustrated that the reinitiation of suppressed convection over the WEIO is preceded by divergence and reduced specific humidity in the boundary layer in situ for about 2 days. Further analysis demonstrates that this reduction of PBL moisture could be primarily attributed to the divergence in the boundary layer rather than the surface latent heat flux, suggesting that this reinitiation process is mainly caused by internal atmospheric dynamics rather than the air–sea interaction process. The decrease of the moisture in the PBL leads to convectively stable stratification and thus suppressed convection.

To understand the mechanism involved during this reinitiation process, or more specifically, to explain how the PBL divergence over the WEIO is generated, an anomalous AGCM is employed. In the model, convective heating over the EEIO is specified based on the composite OLR at the reinitiation phase. In the experiment with a resting environmental flow, a low-level divergence field can be discerned over an elongated region of the WEIO and Africa, resulting from the weakening of westerly zonal flow to the west of the heating. This divergence, however, bears an amplitude one order of magnitude (10^{-8} s^{-1}) smaller than the observed (10^{-7} s^{-1}). In an experiment with the realistic summer mean flow, a stronger divergence perturbation emerges

over the WEIO with a magnitude comparable with the observed, which indicates that this low-level divergence is primarily caused by the ISO convection–mean flow interaction, while the process associated with the decaying of the Rossby wave response may play a minor role.

The diagnosis based on the experiment with summer mean flow indicates that the low-level cold horizontal temperature advection holds a key for the generation of the PBL divergence in situ during the reinitiation phase of suppressed convection over the WEIO. The step-by-step processes involved during the BSISO cycle as revealed by the composite analysis and numerical study can be described as follows:

- After initiated in the WEIO, the enhanced BSISO convection propagates into the EEIO and intensifies. In response to this strong convective heating, southwesterly cross-equatorial winds and asymmetric negative perturbation temperature gradient develop in the lower troposphere over the WEIO due to the modulation of the Gill response by asymmetric 3D summer mean flow.
- The advection of cold mean temperature by the northward perturbation winds and the advection of cold perturbation temperature by the monsoonal mean flow (Somali Jet) lead to the formation of a cold temperature advection center in the lower troposphere over the WEIO.
- During the reinitiation period, perturbation diabatic heating is negligible over the WEIO. Thus, the cold temperature advection is primarily compensated for by the adiabatic warming through the induced perturbation downward motion at the top of the PBL.
- This downward motion and associated PBL divergence further lead to the reduction of the PBL moisture and thus increase the convective stability and finally bring a suppressed convective phase in the WEIO.
- As this suppressed convection intensifies and propagates eastward into the EEIO, a process with an opposite phase repeats. As a result, an enhanced convective phase tends to develop over the WEIO; so on and so forth, the BSISO oscillation continues.

The processes above reveal a self-sustained scenario for the BSISO in the tropical Indian Ocean. The notion that the BSISO appears to be a basinwide phenomenon is also suggested by Webster et al. (2002) in the Joint Air–Sea Monsoon Interaction Experiment (JASMINE).

The intimate relationship between the low-level horizontal temperature advection and divergence over the WEIO as suggested by the AGCM is also verified based on the observed composite results with use of the NCEP–NCAR reanalysis. It is shown that this low-level horizontal temperature advection leads the PBL divergence by 2 days over the BSISO reinitiation region.

It is interesting to note that the low-level divergence field over the WEIO and eastern Africa demonstrates a three-cell wave pattern in both the observations and model results. This wave pattern seems oriented along the topography over eastern Africa. Our numerical experiment illustrates that the east-most divergence cell, which is responsible for the reinitiation of suppressed convection over the WEIO, is primarily ascribed to the modulation of atmospheric response to the ISO heating over the EEIO by asymmetric summer mean flow. However, the results also indicate that the orographic effect over eastern Africa might enhance the divergence in situ to some degree. Recently, Hsu and Lee (2005) suggest the potential role of the tropical topography on the eastward encircling propagation and reinitiation of the MJO. However, their study focused on the topographic impact on the Kelvin wave circulation. In this study, we emphasize the importance of the Rossby wave response to the ISO convection in the EEIO.

It is also worth noting that the reinitiation of the ISO convection would be preconditioned by the large-scale thermal condition in addition to the divergence perturbation in the PBL. A critical SST of about 27.5°C is found to be the threshold for deep convection at many locations in the Indian and Pacific Oceans by Graham and Barnet (1987) and Waliser et al. (1993). In the late summer (August–September), because of the strong coastal upwelling in the WEIO caused by the Somali Jet, the SST is very low in situ (Webster et al. 1998; Kemball-Cook and Wang 2001). As a result, the reinitiation of convection could be hindered over this region, although the divergence perturbation could still be present by the influence of a previous opposite ISO cycle over the EEIO. By a careful examination of the total ISO events that were selected for the composite analysis, it is found that there indeed exists a small portion of cases, in which the reinitiation of new convection cycle tends to take place over the EEIO instead of the WEIO, exhibiting a different behavior as depicted by the general picture in Fig. 3. For these ISO cases, the reinitiation of the new enhanced/suppressed convection phase tends to be connected with the meridional bifurcation of previous suppressed/enhanced convection to the west of the Maritime Continent. Further investigation is needed in order to obtain a better understanding of the complexity of the ISO reinitiation behavior.

On the other hand, why the BSISO convection tends to intensify so rapidly after its reinitiation over the WEIO is not yet completely understood. What processes are involved contributing to this unstable mode? Moreover, the potential impacts of the convection condition over the western Pacific as well as the Indian subcontinent on the ISO reinitiation over the equatorial Indian Ocean are also warranted for further study.

Acknowledgments. The authors thank Dr. Bin Wang and anonymous reviewers for constructive suggestions and comments that led to great improvement of this manuscript. Comments given by Drs. Shang-Ping Xie and Fei-Fei Jin are also greatly appreciated. This work is a part of XJ's Ph.D. dissertation supported partially by the International Pacific Research Center (IPRC). TL acknowledges the support of NSF Grant ATM-0329531. The IPRC is sponsored in part by the Frontier Research System for Global Change.

APPENDIX

Princeton AGCM (Held and Suarez 1984)

The model is a primitive equation model based on the σ coordinate. The prognostic equations are those for the momentum, temperature, and log-surface pressure. Geopotential height and σ-coordinate vertical velocity are calculated from the hydrostatic balance and mass continuity equation. The basic equations can be written as follows:

$$\frac{\partial \mathbf{V}}{\partial t} = -(\zeta + f)\hat{k} \times \mathbf{V} - \dot{\sigma}\frac{\partial \mathbf{V}}{\partial \sigma} - \nabla(\phi + E) + RT\nabla \ln P_s - \varepsilon_1 \mathbf{V} - \upsilon_1 \nabla^4 \mathbf{V}, \quad \text{(A1)}$$

$$\frac{\partial T}{\partial t} = -\mathbf{V} \cdot \nabla T - \dot{\sigma}\frac{\partial T}{\partial \sigma} + kT\left[(\mathbf{V} - \tilde{\mathbf{V}}) \cdot \nabla \ln P_s + \frac{\dot{\sigma}}{\sigma} - \overline{D}\right] + \frac{\dot{Q}}{C_p} - \varepsilon_2 T - \upsilon_2 \nabla^4 T, \quad \text{(A2)}$$

$$\frac{\partial \ln P_s}{\partial t} = -\tilde{D} - \tilde{\mathbf{V}} \cdot \nabla \ln P_s, \quad \text{(A3)}$$

$$\frac{\partial \phi}{\partial \sigma} = -\frac{RT}{\sigma}, \quad \text{(A4)}$$

$$\dot{\sigma} = -\int_0^\sigma \{(D - \tilde{D}) + (\mathbf{V} - \tilde{\mathbf{V}})\nabla \ln P_s\}\, d\sigma, \quad \text{(A5)}$$

where $\mathbf{V}$ is the horizontal vector wind with the zonal component u and meridional component υ; T, $\ln P_s$, D, ϕ, and $\dot{\sigma}$ are temperature, log surface pressure, divergence, geopotential height, and sigma coordinate vertical velocity, respectively; $E = \frac{1}{2}(u^2 + \upsilon^2)$, $k = R/C_p$, and $\dot{Q}$ is the diabatic heating rate. The tildes represent the vertical average. Here ε_1 and ε_2 are the Rayleigh friction and Newtonian cooling coefficients, respectively, and υ_1 and υ_2 are the biharmonic diffusion coefficients for the momentum and temperature. All other notations are standard. The dissipation and diffusion used in the model are described in the text. The momentum equation is transformed to vorticity–divergence form when conducting the integration in the model.

REFERENCES

Annamalai, H., and K. R. Sperber, 2005: Regional heat sources and the active and break phases of boreal summer intraseasonal (30–50 day) variability. *J. Atmos. Sci.,* **62,** 2726–2748.

Bhat, G. S., and Coauthors, 2001: BOBMEX—The Bay of Bengal Monsoon Experiment. *Bull. Amer. Meteor. Soc.,* **82,** 2217–2243.

Bladé, I., and D. L. Hartmann, 1993: Tropical intraseasonal oscillation in a simple nonlinear model. *J. Atmos. Sci.,* **50,** 2922–2939.

Cadet, D. L., 1986: Fluctuations of precipitable water over the Indian Ocean. *Tellus,* **38A,** 170–177.

Chang, C.-P., 1977: Viscous internal gravity waves and low-frequency oscillations in the tropics. *J. Atmos. Sci.,* **34,** 901–910.

——, and H. Lim, 1988: Kelvin wave-CISK: A possible mechanism for the 30–50 day oscillation. *J. Atmos. Sci.,* **45,** 1709–1720.

Ferranti, L., T. N. Palmer, F. Molteni, and K. Klinker, 1990: Tropical–extratropical interaction associated with the 30–60 day oscillation and its impact on medium and extended range prediction. *J. Atmos. Sci.,* **47,** 2177–2199.

Fu, X., B. Wang, T. Li, and J. P. McCreary, 2003: Coupling between northward-propagating, intraseasonal oscillations and sea surface temperature in the Indian Ocean. *J. Atmos. Sci.,* **60,** 1733–1753.

Gadgil, A., and G. Asha, 1992: Intraseasonal variations of the Indian summer monsoon. Part I: Observational aspects. *J. Meteor. Soc. Japan,* **70,** 517–527.

Gill, A. E., 1980: Some simple solutions for heat-induced tropical circulation. *Quart. J. Roy. Meteor. Soc.,* **106,** 447–462.

Graham, N., and T. P. Barnet, 1987: Observations of sea surface temperature and convection over tropical oceans. *Science,* **238,** 657–659.

Hartmann, D. L., M. L. Michelsen, and S. A. Klein, 1992: Seasonal variations of tropical intraseasonal oscillations: A 20–25-day oscillation in the western Pacific. *J. Atmos. Sci.,* **49,** 1277–1289.

Held, I. M., and M. J. Suarez, 1994: A proposal for the intercomparison of the dynamical cores of atmospheric general circulation models. *Bull. Amer. Meteor. Soc.,* **75,** 1825–1830.

Hendon, H., 1988: A simple model of the 40–50 day oscillation. *J. Atmos. Sci.,* **45,** 569–584.

——, and M. L. Salby, 1994: The life cycle of the Madden–Julian oscillation. *J. Atmos. Sci.,* **51,** 2207–2219.

——, C. Zhang, and J. D. Glick, 1999: Interannual variation of the Madden-Julian oscillation during austral summer. *J. Climatol.,* **12,** 2538–2550.

Hsu, H.-H., and M. Lee, 2005: Topographic effects on the eastward propagation and initiation of the Madden–Julian oscillation. *J. Climate,* **18,** 795–809.

——, B. J. Hoskins, and F.-F. Jin, 1990: The 1985/86 intraseasonal oscillation and the role of the extratropics. *J. Atmos. Sci.,* **47,** 823–839.

Hu, Q., and D. A. Randall, 1994: Low-frequency oscillation in radiative–convective systems. *J. Atmos. Sci.,* **51,** 1089–1099.

Jiang, X., T. Li, and B. Wang, 2004: Structures and mechanisms of the northward propagating boreal summer intraseasonal oscillation. *J. Climate,* **17,** 1022–1039.

Julian, P. R., and R. A. Madden, 1981: Comments on a paper by T. Yasunari: A quasistationary appearance of 30- to 40-day period in the cloudiness fluctuations during the summer monsoon over India. *J. Meteor. Soc. Japan,* **59,** 435–437.

Kalnay, E., and Coauthors, 1996: The NCEP/NCAR 40-Year Reanalysis Project. *Bull. Amer. Meteor. Soc.,* **77,** 437–471.

Kemball-Cook, S., 1999: The onset of convection in the Madden-Julian oscillation. Ph.D. thesis, University of California, Davis, 109 pp.

——, and B. Wang, 2001: Equatorial waves and air–sea interaction in the boreal summer intraseasonal oscillation. *J. Climate,* **14,** 2923–2942.

Krishnamurti, T. N., and D. Subrahmanyam, 1982: The 30–50-day mode at 850 mb during MONEX. *J. Atmos. Sci.,* **39,** 2088–2095.

Lau, K.-M., and P. H. Chan, 1986: Aspects of the 40–50 day oscillation during the northern summer as inferred from outgoing longwave radiation. *Mon. Wea. Rev.,* **114,** 1354–1367.

——, and L. Peng, 1987: Origin of low-frequency (intraseasonal) oscillations in the tropical atmosphere. Part I: Basic theory. *J. Atmos. Sci.,* **44,** 950–972.

Lawrence, D. M., and P. J. Webster, 2001: Interannual variations of the intraseasonal oscillation in the south Asian summer monsoon region. *J. Climate,* **14,** 2910–2922.

——, and ——, 2002: The boreal summer intraseasonal oscillation: Relationship between northward and eastward movement of convection. *J. Atmos. Sci.,* **59,** 1593–1606.

Li, T., and B. Wang, 1994: The influence of sea surface temperature on the tropical intraseasonal oscillation: A numerical experiment. *Mon. Wea. Rev.,* **122,** 2349–2362.

Liebmann, B., and C. A. Smith, 1996: Description of a complete (interpolated) outgoing longwave radiation dataset. *Bull. Amer. Meteor. Soc.,* **77,** 1275–1277.

Lorenc, A. C., 1984: The evolution of planetary scale 200 mb divergences during the FGGE year. *Quart. J. Roy. Meteor. Soc.,* **110,** 427–441.

Madden, R. A., and P. R. Julian, 1971: Detection of a 40–50 day oscillation in the zonal wind in the tropical Pacific. *J. Atmos. Sci.,* **28,** 702–708.

——, and ——, 1972: Description of global-scale circulation cells in the tropics with a 40–50 day period. *J. Atmos. Sci.,* **29,** 3138–3158.

——, and ——, 1994: Observations of the 40–50-day tropical oscillation—A review. *Mon. Wea. Rev.,* **122,** 814–837.

Matthews, A. J., 2000: Propagation mechanisms for the Madden-Julian oscillation. *Quart. J. Roy. Meteor. Soc.,* **126,** 2637–2651.

——, and G. N. Kiladis, 1999: The tropical–extratropical interaction between high-frequency transients and the Madden–Julian oscillation. *Mon. Wea. Rev.,* **127,** 661–677.

Murakami, T., T. Nakazawa, and J. He, 1984: On the 40–50 day oscillations during the 1979 Northern Hemisphere summer. I: Phase propagation. *J. Meteor. Soc. Japan,* **62,** 440–468.

Sengupta, D., and M. Ravichandran, 2001: Oscillations of Bay of Bengal sea surface temperature during the 1998 summer monsoon. *Geophys. Res. Lett.,* **28,** 2033–2036.

——, B. N. Goswami, and B. Senan, 2001: Coherent intraseasonal oscillations of ocean and atmosphere during the Asian summer monsoon. *Geophys. Res. Lett.,* **28,** 4127–4130.

Seo, K. H., and K. Y. Kim, 2003: Propagation and initiation mechanisms of the Madden-Julian oscillation. *J. Geophys. Res.,* **108,** 4384, doi:10.1029/2002JD002876.

Sikka, D. R., and S. Gadgil, 1980: On the maximum cloud zone and the ITCZ over Indian longitudes during the southwest monsoon. *Mon. Wea. Rev.,* **108,** 1840–1853.

Slingo, J. M., D. P. Rowell, K. R. Sperber, and F. Norley, 1999: On the predictability of the interannual behaviour of the Madden-Julian Oscillation and its relationship with El Niño. *Quart. J. Roy. Meteor. Soc.,* **125,** 583–606.

Teng, H., and B. Wang, 2003: Interannual variations of the boreal summer intraseasonal oscillation in the Asian–Pacific region. *J. Climate,* **16,** 3572–3584.

Ting, M., and L. Yu, 1998: Steady response to tropical heating in wavy linear and nonlinear baroclinic models. *J. Atmos. Sci.,* **55,** 3565–3582.

Waliser, D. E., N. E. Graham, and C. Gautier, 1993: Comparison of the highly reflective cloud and outgoing longwave radiation datasets for use in estimating tropical deep convection. *J. Climate,* **6,** 331–353.

——, and Coauthors, 2003: AGCM simulations of intraseasonal variability associated with the Asian summer monsoon. *Climate Dyn.,* **21,** 423–446.

Wang, B., and H. Rui, 1990: Synoptic climatology of transient tropical intraseasonal convection anomalies: 1975–1985. *Meteor. Atmos. Phys.,* **44,** 43–61.

——, and T. Li, 1994: Convective interaction with boundary layer dynamics in the development of a tropical intraseasonal system. *J. Atmos. Sci.,* **51,** 1386–1400.

——, and X. Xie, 1996: Low-frequency equatorial waves in vertically sheared zonal flow. Part I: Stable waves. *J. Atmos. Sci.,* **53,** 449–467.

——, and ——, 1997: A model for the boreal summer intraseasonal oscillation. *J. Atmos. Sci.,* **54,** 72–86.

——, R. Wu, and T. Li, 2003: Atmosphere–warm ocean interaction and its impact on Asian–Australian monsoon variation. *J. Climate,* **16,** 1195–1211.

Wang, Z., 2000: The response of the tropical atmosphere to diabatic heating: Effects of the boundary layer and mean flows. M.S. thesis, Dept. of Meteorology, University of Hawaii at Manoa, 51 pp.

Webster, P. J., 1983: Mechanisms of low-frequency variability: Surface hydrological effects. *J. Atmos. Sci.,* **40,** 2110–2124.

——, V. O. Maganã, T. N. Palmer, J. Shukla, R. A. Tomas, M. Yanai, and T. Yasunari, 1998: Monsoons: Processes, predictability, and the prospects for prediction. *J. Geophys. Res.,* **103,** 14 451–14 510.

——, and Coauthors, 2002: The JASMINE pilot study. *Bull. Amer. Meteor. Soc.,* **83,** 1603–1629.

Yasunari, T., 1979: Cloudiness fluctuations associated with the Northern Hemisphere summer monsoon. *J. Meteor. Soc. Japan,* **57,** 227–242.

——, 1980: A quasi-stationary appearance of 30- to 40-day period in the cloudiness fluctuations during the summer monsoon over India. *J. Meteor. Soc. Japan,* **58,** 225–229.

Zhang, C., and H. H. Hendon, 1997: Propagating and standing components of the intraseasonal oscillation in tropical convection. *J. Atmos. Sci.,* **54,** 741–752.

Zhu, B., and B. Wang, 1993: The 30–60-day convection seesaw between the tropical Indian and western Pacific Oceans. *J. Atmos. Sci.,* **50,** 184–199.